Magnetic properties of bilayer triangular lattice

F. M. Hu,[1] S. Q. Su,[1] T. X. Ma,[1,2] and H. Q. Lin[1]
[1]*Department of Physics and Institute of Theoretical Physics, The Chinese University of Hong Kong, Hong Kong, China*
[2]*Max-Planck-Institut für Physik Komplexer Systeme, Nöthnitzer Strasse 38, 01187 Dresden, Germany*
(Received 28 March 2009; revised manuscript received 1 July 2009; published 27 July 2009)

This paper mainly studies the ferromagnetic fluctuations of two types of bilayer triangular lattices on the basis of single-band Hubbard model. First, according to the tight-binding model, energy spectrum, the density of states and spin susceptibility can be obtained analytically. Second, we take finite Coulomb interaction into account, apply the random-phase approximation and do the determinant quantum Monte Carlo simulation. Finally, this paper makes comparisons of magnetic properties of two types of bilayer triangular lattices, and the effects of the interlayer coupling are also discussed in detail.

DOI: 10.1103/PhysRevB.80.014428 PACS number(s): 71.10.Fd, 71.27.+a, 74.20.Mn, 75.40.Mg

I. INTRODUCTION

Recent discovery of superconductivity in $Na_xCoO_2 \cdot yH_2O$ (Ref. 1) and related fascinating normal-state properties[2–4] have revived people's interest in geometrically frustrated systems, such as triangular layers. Although the single-band Hubbard model has been widely studied and understood, it can still be used as the minimum theoretical model when we investigate electron correlations on the two-dimensional triangular lattice. As a starting point, the single-band Hubbard model also helps us study the mechanisms of magnetic fluctuations and superconductivity induced by electron-electron interactions. Previously, the Hubbard model on the single-layer triangular lattice has been studied with various techniques: such as the one-loop renormalization group[5] and the fluctuation exchange approaches.[6] Antiferromagnetic (AFM) correlations near the half filling and ferromagnetic (FM) fluctuations near the van Hove singularity were studied by the determinant quantum Monte Carlo (DQMC) and constrain path Monte Carlo (CPMC) methods, respectively.[7,8]

$Na_xCoO_2 \cdot yH_2O$ has a multilayer structure, and in this system, the distance and couplings between the two CoO_2 layers depend on the inserted H_2O molecules, which are of great interest from both chemical and physical points of view.[9–12] They are also key to understand the pairing mechanism. To address the influences of H_2O molecules between the two CoO_2 layers, it is worth the effort to study the single-band Hubbard model on the bilayer triangular lattices. Previously, electronic structures of cobalt oxide bilayer hydrate were studied by the first-principles calculations.[13] Quantum phase transition was also discussed in the content of the Heisenberg model on the bilayer triangular lattices.[14] For related researches, there are studies of the single-band Hubbard model on bilayer square lattices.[15,16]

In reality, many materials discuss the structures of bilayer triangular lattice, for example, spin-dimer materials $Ba_3Mn_2O_8$ (Refs. 17–19) and Mn_6 molecules,[20] where Mn ions form the bilayer triangular lattice. Another interesting material is graphene, which has attracted great attention recently due to its Dirac fermionic behavior at low energy.[21] Graphene has honeycomb lattice, which can be regarded as two interpenetrating triangular sublattices, and it is similar to the bilayer triangular lattices we are interested in. Here, interlayer coupling plays an important role in these systems.

In this work, we study two types of bilayer triangular lattices as shown in Fig. 1. In Fig. 1(a), for every atom, there are six nearest neighbors in one layer and three next-nearest neighbors in the other layer. This structure is similar to the honeycomb lattice. For the structure shown in Fig. 1(b), every atom has only one next-nearest neighbor in the other layer. We call the lattice shown in Fig. 1(a) structure A and in Fig. 1(b) structure B in all the following. These two structures can be regarded as two-dimensional triangular lattices with every unit cell consisting of two atoms. The model Hamiltonian of the system is

$$H = -t \sum_{\langle \mathbf{i},\mathbf{j}\rangle d\sigma} (c^{\dagger}_{\mathbf{j}d\sigma} c_{\mathbf{i}d\sigma} + \text{H.c.}) - t' \sum_{\langle \mathbf{i},\mathbf{j}\rangle \sigma} (c^{\dagger}_{\mathbf{j}1\sigma} c_{\mathbf{i}2\sigma} + \text{H.c.}) + U \sum_{\mathbf{i}d} n_{\mathbf{i}d\uparrow} n_{\mathbf{i}d\downarrow} - \mu \sum_{\mathbf{i}d\sigma} n_{\mathbf{i}d\sigma}, \quad (1)$$

where $c_{\mathbf{i}d\sigma}$ ($c^{\dagger}_{\mathbf{i}d\sigma}$) annihilates (creates) electrons at site $R_{\mathbf{i}}$ in the dth layer ($d=1,2$) with spin σ ($\sigma=\uparrow,\downarrow$) and $n_{\mathbf{i}d\sigma} = c^{\dagger}_{\mathbf{i}d\sigma} c_{\mathbf{i}d\sigma}$. This system has intralayer nearest-neighbor hopping t and interlayer next-nearest-neighbor hopping t'. These two layers have the same chemical potential μ. We also consider the electron-electron Coulomb interaction U.

Metallic ferromagnetism in correlated systems is a long-standing issue, which has been actively studied both numerically and analytically.[22–25] It has been quite well known that the geometry of the system, the shape of the density of states (DOS), and the large degeneracy of single-particle energy

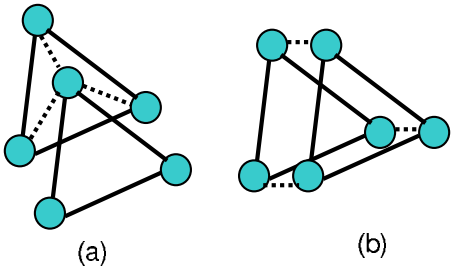

FIG. 1. (Color online) Two types of bilayer triangular lattices studied in this work are shown as structure A in (a) and structure B in (b).

level are crucial to the stability of the FM state.[26–28] The triangular lattice, compared to square lattice, has a higher degeneracy on the energy level and asymmetric distribution of the DOS, so it favors stronger FM fluctuation in some parameter regions. For the single-layer triangular lattice, its DOS has one van Hove singularity at band filling $\langle n\rangle=1.5$. When the interlayer hopping t' is introduced, two van Hove singularities appear with DOS decreasing (see below). According to the itinerant electron FM theory, the FM fluctuations tend to the higher DOS on the Fermi surface. So the interlayer hopping t' will influence the FM fluctuations, which motivates us to compare the spin susceptibilities of single layer with bilayer triangular lattices.

This paper is organized as follows. In Sec. II we calculate the dispersion relations and the DOS for the two types of bilayer triangular lattices at noninteracting limit ($U=0$ refers to as the tight-binding model). The purpose is to study the special feature introduced by the two different structures: one with a finite gap, while the other is gapless, but both of them have two van Hove singularities, which affect their magnetic properties. In Sec. III, the spin susceptibility is studied by applying the random-phase approximation (RPA) to estimate the critical value of Coulomb interaction U_C at which the magnetic instability occurs. Then we obtain a rough estimation before nonperturbative approach is used to deal with electron-electron correlations. In Sec. IV we present numerical results obtained by the DQMC method. For example, we study the FM fluctuation of the system near one of the van Hove singularities in band filling region $1.6\leq n\leq 1.85$. In Sec. V we summarize our results.

II. TIGHT-BINDING MODEL ON THE BILAYER TRIANGULAR LATTICES

To gain some primary insights of the two structures, we begin with investigating their dispersions and DOS and then compare them with the single-layer case. At $U=0$ the tight-binding model Hamiltonian can be diagonalized by using the Fourier transformation

$$c_{\mathbf{i}d\sigma}=\frac{1}{\sqrt{N}}\sum_{\mathbf{k}} e^{i\mathbf{k}\cdot R_{\mathbf{i}}}c_{\mathbf{k}d\sigma},$$

$$c^{\dagger}_{\mathbf{i}d\sigma}=\frac{1}{\sqrt{N}}\sum_{\mathbf{k}} e^{-i\mathbf{k}\cdot R_{\mathbf{i}}}c^{\dagger}_{\mathbf{k}d\sigma}.$$

Then the Hamiltonian has a simple form of sum of 2×2 matrices,

$$H=\sum_{\mathbf{k}\sigma}(c^{\dagger}_{\mathbf{k}1\sigma}\quad c^{\dagger}_{\mathbf{k}2\sigma})\begin{pmatrix}\alpha_{\mathbf{k}} & \beta_{\mathbf{k}}\\ \beta^{*}_{\mathbf{k}} & \alpha_{\mathbf{k}}\end{pmatrix}\begin{pmatrix}c_{\mathbf{k}1\sigma}\\ c_{\mathbf{k}2\sigma}\end{pmatrix}. \tag{2}$$

The elements of the 2×2 matrix are

$$\alpha_{\mathbf{k}}=-2t[\cos\mathbf{k}\cdot\vec{a_1}+\cos\mathbf{k}\cdot\vec{a_2}+\cos\mathbf{k}\cdot(\vec{a_1}-\vec{a_2})]-\mu,$$

$$\beta_{\mathbf{k}}=-t'[1+e^{i\mathbf{k}\cdot(\vec{a_1}-\vec{a_2})}+e^{-i\mathbf{k}\cdot\vec{a_2}}].$$

The 2×2 matrix can be diagonalized by the following linear transformation:

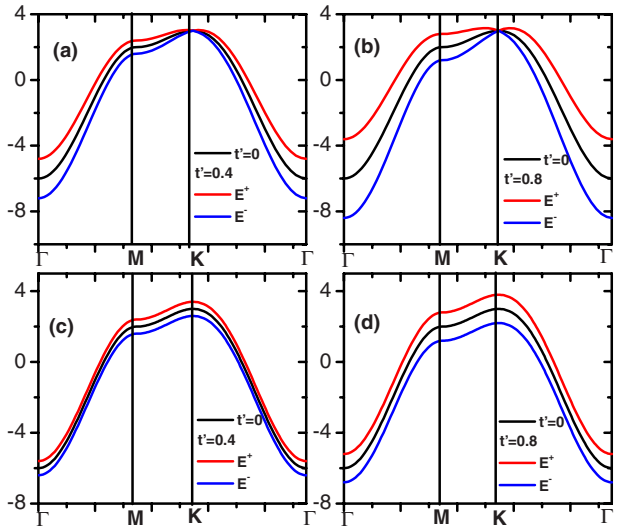

FIG. 2. (Color online) Dispersion relations for structure A are represented in (a) and (b), while (c) and (d) represent structure B. In every subfigure the upper curves represent the band E^{+}, the middle curves represent single-layer triangular lattice $t'=0$, and the lower curves represent band E^{-}.

$$c_{\mathbf{k}1\sigma}=\frac{\sqrt{2}}{2}\frac{|\beta_{\mathbf{k}}|}{\beta^{*}_{\mathbf{k}}}(d_{\mathbf{k}1\sigma}+d_{\mathbf{k}2\sigma}), \tag{3a}$$

$$c_{\mathbf{k}2\sigma}=\frac{\sqrt{2}}{2}(d_{\mathbf{k}1\sigma}-d_{\mathbf{k}2\sigma}), \tag{3b}$$

where we introduced another set of operators $d_{\mathbf{k}1\sigma}$ and $d_{\mathbf{k}2\sigma}$. Then the Hamiltonian has the diagonalized form as

$$H=\sum_{\mathbf{k}\sigma}(E^{+}d^{\dagger}_{\mathbf{k}1\sigma}d_{\mathbf{k}1\sigma}+E^{-}d^{\dagger}_{\mathbf{k}2\sigma}d_{\mathbf{k}2\sigma}). \tag{4}$$

Because of double layers, the energy spectrum has two bands. For structure A,

$$E^{\pm}_{\mathbf{k}}=-tG(\mathbf{k})-\mu\pm t'\sqrt{3+G(\mathbf{k})}, \tag{5}$$

while for structure B,

$$E^{\pm}_{\mathbf{k}}=-tG(\mathbf{k})-\mu\pm t'. \tag{6}$$

Here,

$$G(\mathbf{k})=2[\cos\mathbf{k}\cdot\vec{a_1}+\cos\mathbf{k}\cdot\vec{a_2}+\cos\mathbf{k}\cdot(\vec{a_1}-\vec{a_2})]. \tag{7}$$

Figure 2 represents the dispersion relations for the two structures along the symmetry path in the first Brillouin zone (BZ). Following the convention, **Γ** point is (0,0), **M** point is $(0,\pi)$, and **K** point is $(-\frac{2\pi}{3},\frac{2\pi}{3})$. We calculate the dispersion relations for $t'=0$ (the case of single layer), $t'=0.4$, and $t'=0.8$ (unit of t). The effects of t' are evident: (1) for structure A, there is no gap between the two bands, while for structure B, there is an energy gap equal to $2t'$ at **K** point. At finite temperatures, the electrons will occupy not only lower band but also upper band, so this energy gap will affect correlations between the two bands; (2) the bandwidth of spectrum becomes lager when t' increases, so we expect that the Coulomb interaction will have smaller influences on the mag-

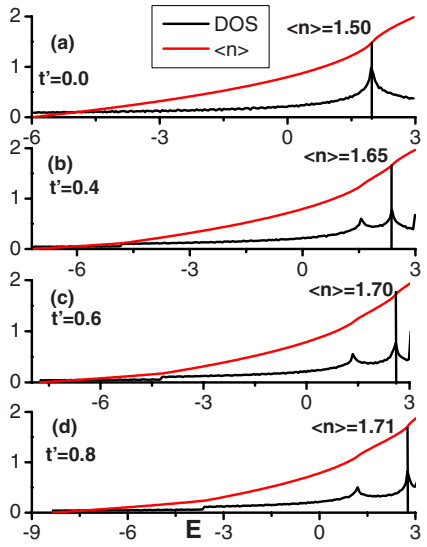

FIG. 3. (Color online) DOS and band fillings of structure A are functions of energy: the red curves represent fillings $\langle n \rangle$ and the black lines represent the DOS computed from Eq. (5). The marked $\langle n \rangle$ are the filling values at one of the van Hove singularities.

netic fluctuations. We also note that, as shown in Fig. 2, there exist saddle points near **K** point, where the DOS has a large value.

In Figs. 3 and 4, in the single-layer triangular lattice case, $t'=0$, there is only one van Hove singularity at filling $\langle n \rangle = 1.5$. When t' is introduced the van Hove singularity becomes two separated peaks, and with t' increasing, one peak moves toward the half filling while the other one toward the full filling. We will study the magnetic properties in the high band filling region. In particular, FM fluctuations may arise due to this higher DOS near the Fermi level.

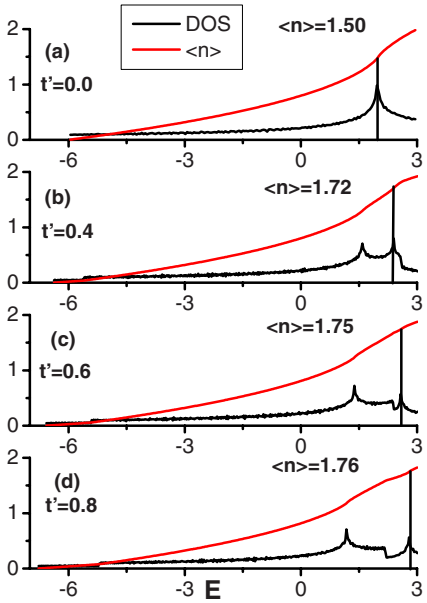

FIG. 4. (Color online) DOS and band fillings of structure B are functions of energy: the red curves represent fillings $\langle n \rangle$ and the black lines represent the DOS computed from Eq. (6). The marked $\langle n \rangle$ are the filling values at one of the van Hove singularities.

Comparing DOS of the two bilayer structures as shown in Figs. 3 and 4, in the high filling region, it is clear that DOS of structure A is larger than that of structure B, in particular their DOS at the van Hove singularities near the band top. In terms of Stoner's FM theory for itinerant electrons, FM fluctuations tend to high DOS on the Fermi surface. So if we locate the Fermi surface near van Hove singularity by adjusting chemical potential, we expect that the magnetic fluctuations are stronger in structure A than that in structure B. These expectations will be tested by the RPA calculations and quantum Monte Carlo simulations, which will be discussed in the following sections.

III. SPIN SUSCEPTIBILITY FOR THE TIGHT-BINDING MODEL

In this section, we calculate the spin susceptibility for the tight-binding model and then apply RPA to estimate critical values of Coulomb interaction when magnetic instabilities occur. The spin susceptibility in the z direction at frequency $\omega=0$ is given by

$$\chi_{dd'}(\mathbf{q}) = \frac{1}{N}\int_0^\beta d\tau \sum_{\mathbf{ij}} e^{i\mathbf{q}\cdot(R_\mathbf{i}-R_\mathbf{j})}\langle m_d^z(R_\mathbf{i},\tau) m_{d'}^z(R_\mathbf{j},0)\rangle, \quad (8)$$

where $m_d^z(R_\mathbf{i},0)=c_{d\mathbf{i}\uparrow}^\dagger c_{d\mathbf{i}\uparrow}-c_{d\mathbf{i}\downarrow}^\dagger c_{d\mathbf{i}\downarrow}$ and $m_d^z(R_\mathbf{i},\tau)=e^{H\tau}m_d^z(R_\mathbf{i},0)e^{-H\tau}$, and N is the number of sites in one layer. The susceptibility has four components, χ_{11}, χ_{12}, χ_{21}, and χ_{22}. Obviously, there exist the relations $\chi_{11}=\chi_{22}$ and $\chi_{12}=\chi_{21}^*$. Because the Hamiltonian is solvable the spin susceptibility can be calculated analytically. After performing Fourier's transformation, there are mean values of several four-operator terms in the spin susceptibility as follows:

$$\frac{1}{N}\int_0^\beta d\tau \sum_{\mathbf{ij}} e^{i\mathbf{q}\cdot(R_\mathbf{i}-R_\mathbf{j})}\langle c_{\mathbf{i}d\sigma}^\dagger(\tau)c_{\mathbf{i}d\sigma}(\tau)c_{\mathbf{j}d'\sigma'}^\dagger c_{\mathbf{j}d'\sigma'}\rangle$$
$$= \frac{1}{N^3}\int_0^\beta d\tau \sum_{\mathbf{ij}}\sum_{\{\mathbf{k}\}}\langle c_{\mathbf{k}_1 d\sigma}^\dagger(\tau)c_{\mathbf{k}_2 d\sigma}(\tau)$$
$$\times c_{\mathbf{k}_3 d'\sigma'}^\dagger c_{\mathbf{k}_4 d'\sigma'}\rangle \cdot e^{i\mathbf{q}\cdot(R_\mathbf{i}-R_\mathbf{j})+i(\mathbf{k}_1-\mathbf{k}_2)\cdot R_\mathbf{i}+i(\mathbf{k}_3-\mathbf{k}_4)\cdot R_\mathbf{j}}, \quad (9)$$

where $c_{\mathbf{i}\sigma}(\tau)=e^{H\tau}c_{\mathbf{i}\sigma}e^{-H\tau}$. By the linear transformation of Eqs. (3a) and (3b), we calculate these correlation functions by applying Wick's theorem. The intralayer spin susceptibility has the form

$$\chi_{11}(\mathbf{q}) = B_1 + B_2 + B_3 + B_4, \quad (10)$$

and the four correlation functions are

$$B_1 = -\frac{1}{4N}\sum_{\mathbf{k},\sigma}\frac{\langle n_{\mathbf{k+q}1\sigma}\rangle - \langle n_{\mathbf{k}1\sigma}\rangle}{E_{\mathbf{k+q}}^+ - E_\mathbf{k}^+}, \quad (11a)$$

$$B_2 = -\frac{1}{4N}\sum_{\mathbf{k},\sigma}\frac{\langle n_{\mathbf{k+q}2\sigma}\rangle - \langle n_{\mathbf{k}1\sigma}\rangle}{E_{\mathbf{k+q}}^- - E_\mathbf{k}^+}, \quad (11b)$$

$$B_3 = -\frac{1}{4N}\sum_{\mathbf{k},\sigma}\frac{\langle n_{\mathbf{k+q}1\sigma}\rangle - \langle n_{\mathbf{k}2\sigma}\rangle}{E_{\mathbf{k+q}}^+ - E_\mathbf{k}^-}, \quad (11c)$$

$$B_4 = -\frac{1}{4N}\sum_{\mathbf{k},\sigma}\frac{\langle n_{\mathbf{k}+\mathbf{q}2\sigma}\rangle - \langle n_{\mathbf{k}2\sigma}\rangle}{E^-_{\mathbf{k}+\mathbf{q}} - E^-_{\mathbf{k}}}. \tag{11d}$$

The interlayer susceptibility also can be written as

$$\chi_{12}(\mathbf{q}) = C_1 + C_2 + C_3 + C_4, \tag{12}$$

there are also four terms as

$$C_1 = -\frac{1}{4N}\sum_{\mathbf{k},\sigma}\frac{\langle n_{\mathbf{k}+\mathbf{q}1\sigma}\rangle - \langle n_{\mathbf{k}1\sigma}\rangle}{E^+_{\mathbf{k}+\mathbf{q}} - E^+_{\mathbf{k}}}e^{i(\varphi_{\mathbf{k}+\mathbf{q}}-\varphi_{\mathbf{k}})}, \tag{13a}$$

$$C_2 = \frac{1}{4N}\sum_{\mathbf{k},\sigma}\frac{\langle n_{\mathbf{k}+\mathbf{q}2\sigma}\rangle - \langle n_{\mathbf{k}1\sigma}\rangle}{E^-_{\mathbf{k}+\mathbf{q}} - E^+_{\mathbf{k}}}e^{i(\varphi_{\mathbf{k}+\mathbf{q}}-\varphi_{\mathbf{k}})}, \tag{13b}$$

$$C_3 = \frac{1}{4N}\sum_{\mathbf{k},\sigma}\frac{\langle n_{\mathbf{k}+\mathbf{q}1\sigma}\rangle - \langle n_{\mathbf{k}2\sigma}\rangle}{E^+_{\mathbf{k}+\mathbf{q}} - E^-_{\mathbf{k}}}e^{i(\varphi_{\mathbf{k}+\mathbf{q}}-\varphi_{\mathbf{k}})}, \tag{13c}$$

$$C_4 = -\frac{1}{4N}\sum_{\mathbf{k},\sigma}\frac{\langle n_{\mathbf{k}+\mathbf{q}2\sigma}\rangle - \langle n_{\mathbf{k}2\sigma}\rangle}{E^-_{\mathbf{k}+\mathbf{q}} - E^-_{\mathbf{k}}}e^{i(\varphi_{\mathbf{k}+\mathbf{q}}-\varphi_{\mathbf{k}})}, \tag{13d}$$

here $\langle n_{\mathbf{k}1(2)}\rangle$ is the occupation number of electrons in band $E^{+(-)}$ with momentum $\mathbf{k}$, and the phase factor $e^{i\varphi_{\mathbf{k}}}=\frac{\beta_{\mathbf{k}}}{|\beta_{\mathbf{k}}|}$. For paramagnetic correlations, the mean value of occupation number obeys Fermi's distribution. First, when $t'=0$ the two bands are the same $E^+(\mathbf{k})=E^-(\mathbf{k})$, and Eq. (10) becomes

$$\chi_{11}(\mathbf{q}) = -\frac{1}{N}\sum_{\mathbf{k},\sigma}\frac{\langle n_{\mathbf{k}+\mathbf{q}\sigma}\rangle - \langle n_{\mathbf{k}\sigma}\rangle}{E_{\mathbf{k}+\mathbf{q}} - E_{\mathbf{k}}},$$

which is well known as the spin susceptibility in the single-band case while $\chi_{12}(\mathbf{q})$ becomes zero. Second, we compare these two correlation functions and observe that χ_{12} has an added phase factor and its four terms have different signs, which result in $\chi_{12}(\mathbf{q})$ being much smaller than $\chi_{11}(\mathbf{q})$. We expect that if the energy gap is larger, the correlation functions decrease and the spin susceptibilities become smaller accordingly. In view of the DOS, when the differences of energy $\Delta E=E_{\mathbf{k}+\mathbf{q}}-E_{\mathbf{k}}$ with given momentum $\mathbf{q}$ (either within one band or between two bands) varies more rapidly, correspondingly, the DOS will be smaller, as well as spin susceptibility.

Figure 5 shows the total spin susceptibilities $\chi_0(\mathbf{q})=\frac{1}{2}\Sigma_{dd'}\chi_{dd'}(\mathbf{q})$ of the tight-binding model at zero frequency for different t'. Corresponding band fillings are marked in Figs. 3 and 4. In Figs. 5(a) and 5(b) the spin susceptibility will increase rapidly when the temperature is lowered, but at $T=1.0$ (unit of t), the curves of susceptibilities are very smooth. It is shown in Figs. 5(c) and 5(d) that spin susceptibilities become smaller as t' increases. We compare the results of the two types of bilayer triangular lattices and find that the spin susceptibility of structure B is lower than that of structure A. It is because that when t' increases, near the van Hove singularity the energy gap of structure B is magnified and the DOS decreases. In structure A the value of $\chi_0(\mathbf{K})$ is not sensitive to the change in t' because the two energy bands are degenerate at **K** point.

When interaction U is turned on, the magnetic susceptibility within RPA is given by[29]

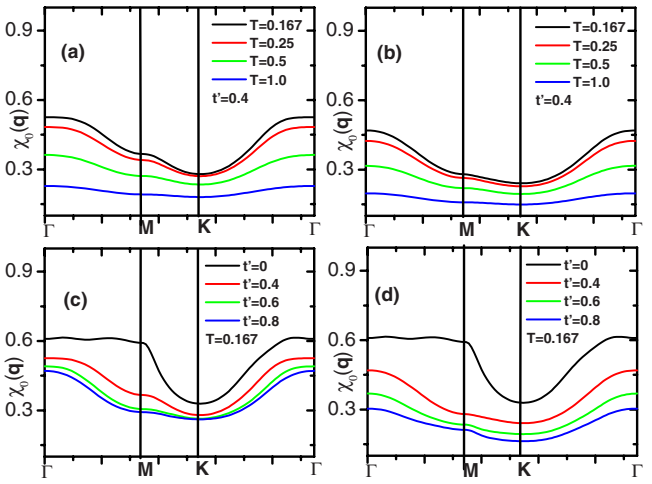

FIG. 5. (Color online) (a) and (c) represent the results of structure A, and (b) and (d) represent the results of structure B. The momentum $\mathbf{q}$ is along $\Gamma\rightarrow\mathbf{M}\rightarrow\mathbf{K}\rightarrow\Gamma$ in the first BZ.

$$\chi(\mathbf{q}) = \frac{\chi_0(\mathbf{q})}{1 - U\chi_0(\mathbf{q})}. \tag{14}$$

Because we are interested in the region far away from the half filling, RPA predicts a transition between paramagnetic phase and FM phase with the high DOS when the critical condition is satisfied,

$$1 - U\chi_0(\mathbf{q}) = 0. \tag{15}$$

At zero temperature, Eq. (15) becomes the Stoner criterion $U\rho(E_F)=1$, where $\rho(E_F)$ is the DOS on the Fermi surface. On one hand when we tune band filling to localize the Fermi energy at the van Hove singularity, the system is unstable against FM fluctuation. On the other hand Eq. (15) can be used to determine the critical strength U_C as the transition appears.

We calculate U_C with given t' and temperatures. First, for the two structures with fixed value of t', U_C decreases as temperature is lowered. Second, when t' is increasing, a larger U_C is needed for the transition between paramagnetic and FM phases. Third, with the same t' and temperature, U_C of structure A is a bit smaller than that of structure B. Moreover we expect that when parameters are the same for the two different systems, the FM fluctuation is stronger in structure A than that in structure B. The results of RPA are reasonable because in Figs. 3 and 4, it is shown that for structure B the region between two singularities is wider and the DOS is lower than those for structure A.

Although the validity of RPA is limited, data presented in Tables I and II are helpful in choosing appropriate parameters for quantum Monte Carlo simulations. In the following section, we will observe that FM fluctuations are noticeable both in structures A and B for certain parameters, but for some parameters the fluctuation in structure B is suppressed.

TABLE I. The critical value U_C (unit of t) for structure A.

U_C	T=0.167	0.25	0.5	1.0
t'=0	1.63	1.82	2.41	3.65
t'=0.4	1.90	2.07	2.76	4.38
t'=0.6	2.05	2.26	3.08	4.90
t'=0.8	2.13	2.39	3.26	5.13

IV. QUANTUM MONTE CARLO ANALYSIS ON THE SPIN SUSCEPTIBILITY

To deal with electron-electron interaction nonperturbatively, we use the DQMC method[30] to simulate the single-band Hubbard model on the bilayer triangular lattices and treat this system as a grand canonical ensemble at finite temperatures. We mainly calculate the spin susceptibility by the unequal-time Green's function in the imaginary-time direction. We perform DQMC simulation on this model for three sizes of lattice, 36×2, 48×2, and 64×2 sites. Simulations were done for both two structures as shown in Fig. 1. In the filling regions under investigation, the behaviors of the spin susceptibilities are qualitatively similar. We present here the results at band filling $\langle n\rangle$=1.7. Figure 6 shows $\chi(\mathbf{q})$ versus momentum $\mathbf{q}$ along the symmetry path in the first BZ for U=8 and T=0.33. The critical values of Coulomb interaction, U_C, based on RPA results (with the same parameters t' and T) in Sec. III, are much smaller than the value we adopt here (U=8). So magnetic fluctuations in the three structures, the single-layer triangular lattices (t'=0), and the two types of bilayer lattices with (t'=0.6), are evident, and in the six subpictures we compare their spin susceptibilities. In both t'=0 and t'=0.6 cases, $\chi(\mathbf{q})$ have broad peaks around the $\mathbf{\Gamma}$ points, indicating obvious FM fluctuations in these systems. Compared to the spin susceptibilities in Fig. 5 it is seen that considerable Coulomb interaction greatly intensifies magnetic fluctuations. Moreover when t' increases, $\chi(\mathbf{0})$ ($\mathbf{\Gamma}$ point) decreases and the FM fluctuations are suppressed. On the coupled bilayer square lattices, the similar results for the AFM fluctuations were reported.[16] We may attribute this phenomenon to the Stoner's theory that the FM fluctuations tend to the high DOS on the Fermi surface. When t' is introduced the original singularity is divided into two peaks; as a result, the DOS near these two peaks is lowered.

In Figs. 7 and 8, we present the spin susceptibilities on the 48×2 and 64×2 lattice, respectively. We fix band filling $\langle n\rangle$=1.7 and U=8, which is about the bandwidth. At temperature T=0.33, it is clear that there are FM fluctuations, but at higher temperature T=1.0, the curves of $\chi(\mathbf{q})$ become much smooth, namely, the FM fluctuations are not noticeable.

TABLE II. The critical value U_C for structure B.

U_C	T=0.167	0.25	0.5	1.0
t'=0	1.63	1.82	2.41	3.65
t'=0.4	2.13	2.36	3.16	5.07
t'=0.6	2.71	2.89	3.74	5.63
t'=0.8	3.29	3.45	4.12	6.00

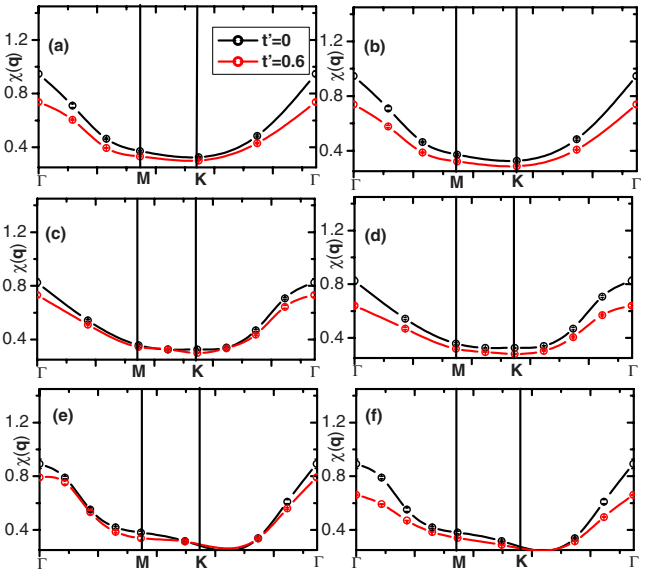

FIG. 6. (Color online) The spin susceptibilities $\chi(\mathbf{q})$ in (a) and (b) are for the 36×2 lattice, in (c) and (d) are for the 48×2 lattice, and in (e) and (f) are for the 64×2 lattice, with parameters U=8, T=0.33, and filling $\langle n\rangle$=1.7. (a), (c), and (e) are for structure A, and (b), (d), and (f) are for structure B. The momentum $\mathbf{q}$ is along $\mathbf{\Gamma}\rightarrow\mathbf{M}\rightarrow\mathbf{K}\rightarrow\mathbf{\Gamma}$ in the first BZ.

In Fig. 9, we study the spin susceptibilities $\chi(\mathbf{q})$ versus t' with U=4 and temperature T=0.25. The band filling $\langle n\rangle$ is fixed at 1.7 with high DOS, as is shown in Figs. 3 and 4. We do the calculations on the 48×2 lattice. To emphasize the effects of t', we also show the results of the single-layer triangular lattices in every subfigure. Figure 9(a) shows the results of structure A, and Fig. 9(b) shows the results of structure B. The rise in $\chi(\mathbf{q})$ with t' decreasing can be seen

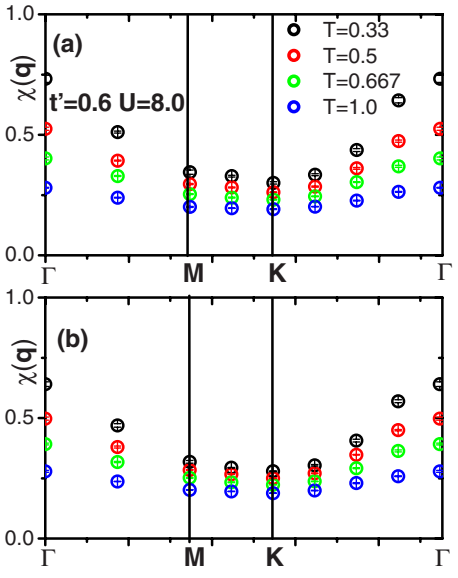

FIG. 7. (Color online) The spin susceptibility $\chi(\mathbf{q})$ is represented versus temperature on the 48×2 lattice with U=8 and filling $\langle n\rangle$=1.7. (a) is for structure A and (b) is for structure B.

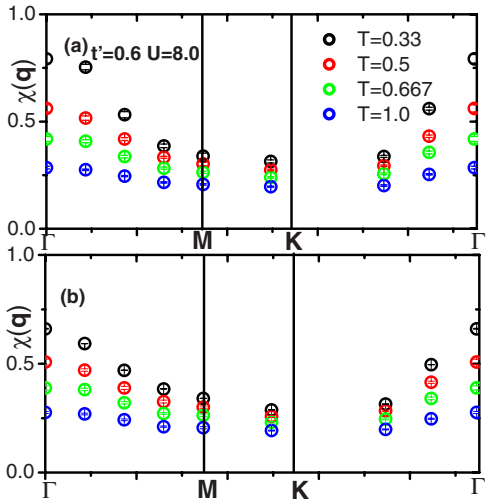

FIG. 8. (Color online) The spin susceptibility $\chi(\mathbf{q})$ is represented versus temperature on the 64×2 lattice with $U=8$ and filling $\langle n\rangle=1.7$. (a) is for structure A, and (b) is for structure B.

to occur in both types of bilayer structures. It is interesting that the values of $\chi(\mathbf{0})$ in structure B decrease more rapidly than that in structure A with t' increasing. Between **M** and **K** points in the first BZ of structure A, the spin susceptibility curves with different t' are close to each other. It is because the two energy bands are degenerate at the **K** point. On the contrary, the structure B with energy gap at this point does not have the same behavior.

With extensive DQMC simulation data, let us compare magnetic properties of the two types of bilayer triangular lattices in detail with Figs. 10–13. We observe that the van Hove singularities for two structures with $t'=0.4$ are localized in the filling regions between 1.6 and 1.75. With $t'=0.8$ the van Hove singularities are in the zones from 1.7 to 1.85. When $t'=0.4$ the spin susceptibility of structure B is little lower than that of structure A on the 48×2 lattice, but this difference is not evident on the 64×2 lattice. When t'

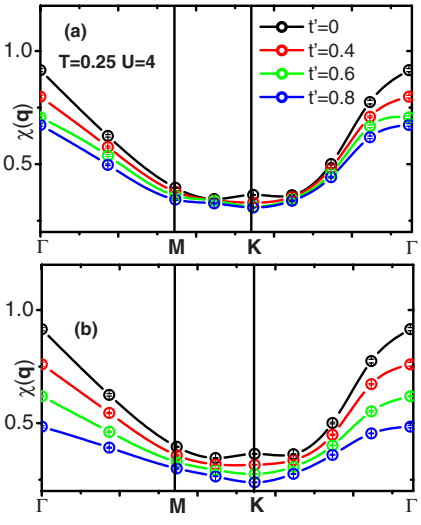

FIG. 9. (Color online) The spin susceptibility $\chi(\mathbf{q})$ is represented versus t' on the 48×2 lattice with filling $\langle n\rangle=1.7$, $U=4$, and $T=0.33$. (a) is for structure A, and (b) is for structure B.

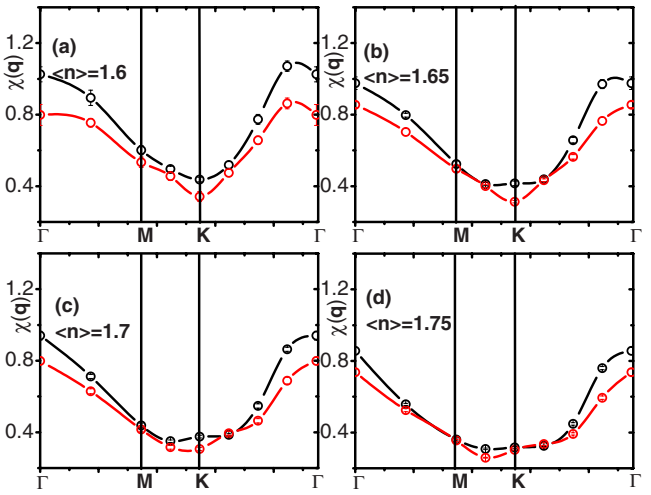

FIG. 10. (Color online) The spin susceptibility $\chi(\mathbf{q})$ is represented versus filling on the 48×2 lattice for $U=4$, $T=0.167$, and $t'=0.4$. The black curves are for structure A, and the red curves are for structure B.

increases to 0.8, the FM fluctuations in structure B decay monotonically but in structure A FM fluctuations are still obvious. We take $U=4$, $T=0.167$, and $t'=0.4$, 0.8. Given the results of RPA in Tables I and II, when $t'=0.4$ the critical values U_C of the two structures are about 2, one-half of the value $(U=4)$ was used in simulations. However when $t'=0.8$, the critical value U_C of structure A is still about 2; but for structure B, U_C approaches 4. In this case, the strength of electron-electron interaction is enough to induce FM fluctuations in structure A but not in structure B.

Figures 10–13 show band filling dependence of $\chi(\mathbf{q})$. For $t'=0.4$ and $\langle n\rangle=1.6$ the peak of $\chi(\mathbf{q})$ near the $\mathbf{\Gamma}$ point is broadened, and when the band filling varies from 1.65 to 1.7 the peak of $\chi(\mathbf{q})$ at $\mathbf{\Gamma}$ point is strengthened; as band filling reaches 1.75 the value of $\chi(\mathbf{0})$ begins to decrease. These phenomena exist in both structures A and B. When $t'=0.8$

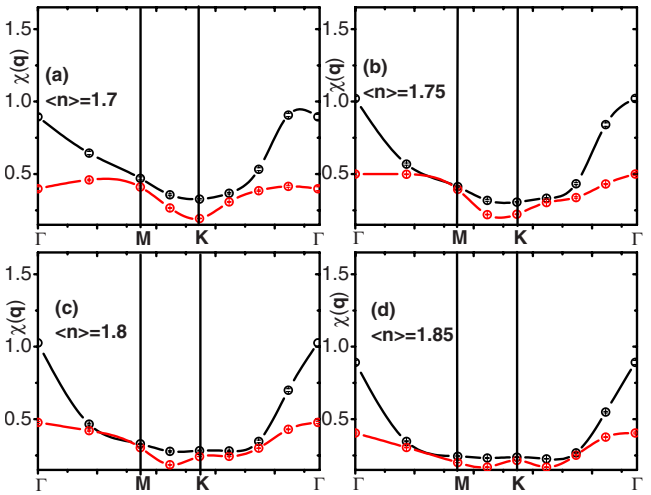

FIG. 11. (Color online) The spin susceptibility $\chi(\mathbf{q})$ is represented versus filling on the 48×2 lattice for $U=4$, $T=0.167$, and $t'=0.8$. The black curves are for structure A, and the red curves are for structure B.

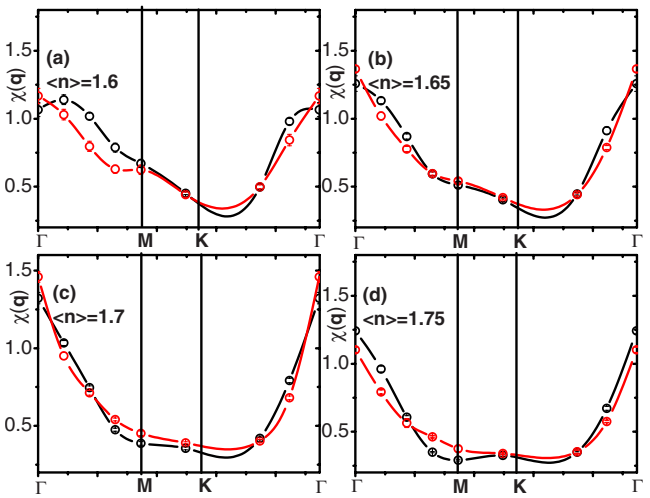

FIG. 12. (Color online) The spin susceptibility $\chi(\mathbf{q})$ is represented versus filling on the 64×2 lattice for $U=4$, $T=0.167$, and $t'=0.4$. The black curves are for structure A, and the red curves are for structure B.

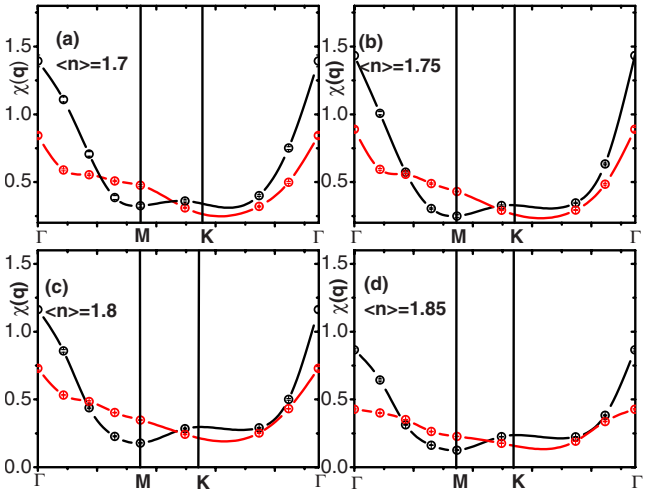

FIG. 13. (Color online) The spin susceptibility $\chi(\mathbf{q})$ is represented versus filling on the 64×2 lattice for $U=4$, $T=0.167$, and $t'=0.8$. The black curves are for structure A, and the red curves are for structure B.

and band filling varies from 1.75 to 1.85 there are very weak FM fluctuations in structure B. In contrast, there are distinct FM fluctuations in structure A, which become the strongest when filling reaches 1.75.

V. CONCLUSION

In this paper we have studied the magnetic properties of two types of bilayer triangular lattices. We calculated the energy spectrum and the DOS based on the tight-binding model. When the interlayer hopping t' is introduced, the spectrum has two bands. The energy bands of structure A are degenerate at **K** point. On the contrary, for structure B, there is a considerable gap between the two bands. Compared to the case of single layer, the DOS of bilayer structure is lower in the filling region $\langle n\rangle=1.5-1.9$. Moreover, there are two singularities in the DOS for the bilayer triangular lattices. By performing the RPA calculations, we obtained the critical values of the Coulomb interaction U_C of the magnetic instability. The results showed that with increasing t', larger U_C is needed. For the same t', structure B requires a larger U_C than that of structure A.

We have carried out a DQMC simulation for the single-band Hubbard model on the bilayer triangular lattices. By calculating the spin susceptibility, we studied the magnetic properties of the bilayer systems near the van Hove singularities. By the itinerant electron magnetism theory, the FM fluctuations tend to the high DOS on the Fermi surface. Compared to the single-layer triangular lattice case, when t' is gradually increasing, FM fluctuations are suppressed in both structures A and B.

We have explained the effects of t' on the FM fluctuations in terms of the DOS. After analyzing the spin susceptibilities with the same t', the conclusion is that the FM fluctuations are weaker in structure B than those in structure A. This helps us in understanding the effects of frustration on the magnetic properties of various structures.

ACKNOWLEDGMENTS

The authors are grateful to Yi Zhou and Yan-Ling Li for helpful discussions. This work is supported by HKSAR RGC (Project No. CUHK 401806).

[1] K. Takada, H. Sakurai, E. Takayama-Muromachi, F. Izumi, R. A. Dilanian, and T. Sasaki, Nature (London) **422**, 53 (2003).
[2] D. J. Singh, Phys. Rev. B **68**, 020503(R) (2003).
[3] K.-W. Lee, J. Kunes, and W. E. Pickett, Phys. Rev. B **70**, 045104 (2004).
[4] P. H. Zhang, W. D. Luo, M. L. Cohen, and S. G. Louie, Phys. Rev. Lett. **93**, 236402 (2004).
[5] C. Honerkamp, Phys. Rev. B **68**, 104510 (2003).
[6] M. M. Korshunov, I. Eremin, A. Shorikov, V. I. Anisimov, M. Renner, and W. Brenig, Phys. Rev. B **75**, 094511 (2007).
[7] N. Bulut, W. Koshibae, and S. Maekawa, Phys. Rev. Lett. **95**, 037001 (2005).
[8] S. Q. Su, Z. B. Huang, R. Fan, and H. Q. Lin, Phys. Rev. B **77**, 125114 (2008).
[9] J. W. Lynn, Q. Huang, C. M. Brown, V. L. Miller, M. L. Foo, R. E. Schaak, C. Y. Jones, E. A. Mackey, and R. J. Cava, Phys. Rev. B **68**, 214516 (2003).
[10] J. D. Jorgensen, M. Avdeev, D. G. Hinks, J. C. Burley, and S. Short, Phys. Rev. B **68**, 214517 (2003).
[11] M. D. Johannes and D. J. Singh, Phys. Rev. B **70**, 014507 (2004).
[12] R. J. Xiao, H. X. Yang, and J. Q. Li, Phys. Rev. B **73**, 092517

(2006).
[13] R. Arita, Phys. Rev. B **71**, 132503 (2005).
[14] R. R. P. Singh and N. Elstner, Phys. Rev. Lett. **81**, 4732 (1998).
[15] R. T. Scalettar, J. W. Cannon, D. J. Scalapino, and R. L. Sugar, Phys. Rev. B **50**, 13419 (1994).
[16] K. Bouadim, G. G. Batrouni, F. Hebert, and R. T. Scalettar, Phys. Rev. B **77**, 144527 (2008).
[17] M. B. Stone, M. D. Lumsden, Y. Qiu, E. C. Samulon, C. D. Batista, and I. R. Fisher, Phys. Rev. B **77**, 134406 (2008).
[18] E. C. Samulon, Y.-J. Jo, P. Sengupta, C. D. Batista, M. Jaime, L. Balicas, and I. R. Fisher, Phys. Rev. B **77**, 214441 (2008).
[19] M. B. Stone, M. D. Lumsden, S. Chang, E. C. Samulon, C. D. Batista, and I. R. Fisher, Phys. Rev. Lett. **100**, 237201 (2008).
[20] S. Bahr, C. J. Milios, L. F. Jones, E. K. Brechin, V. Mosser, and W. Wernsdorfer, Phys. Rev. B **78**, 132401 (2008).
[21] K. S. Novoselov, A. K. Geim, S. V. Morozov, D. Jiang, M. I. Katsnelson, I. V. Grigorieva, S. V. Dubonos, and A. A. Firsov, Nature (London) **438**, 197 (2005).
[22] H. Tasaki, Phys. Rev. Lett. **73**, 1158 (1994).
[23] R. Hlubina, S. Sorella, and F. Guinea, Phys. Rev. Lett. **78**, 1343 (1997).
[24] S. Daul and R. M. Noack, Phys. Rev. B **58**, 2635 (1998).
[25] T. Wegner, M. Potthoff, and W. Nolting, Phys. Rev. B **57**, 6211 (1998).
[26] L. Arrachea, Phys. Rev. B **62**, 10033 (2000).
[27] T. Koretsune and M. Ogata, J. Phys. Soc. Jpn. **72**, 2437 (2003).
[28] H. Q. Lin and J. E. Hirsch, Phys. Rev. B **35**, 3359 (1987).
[29] S. Doniach and E. Sondheimer, *Green's Function for Solid State Physicists* (Benjamin, Reading, MA, 1982).
[30] R. Blankenbecler, D. J. Scalapino, and R. L. Sugar, Phys. Rev. D **24**, 2278 (1981).